Enhancing Inverse Halftoning via Coupled Dictionary Training

Pedro G. Freitas, Mylène C.Q. Farias, Aletéia P.F. Araújo

www.elsevier.com/locate/image

PII: S0923-5965(16)30142-4
DOI: http://dx.doi.org/10.1016/j.image.2016.09.008
Reference: IMAGE15136

To appear in: *Signal Processing : Image Communication*

Received date: 6 May 2016
Revised date: 27 September 2016
Accepted date: 27 September 2016

Cite this article as: Pedro G. Freitas, Mylène C.Q. Farias and Aletéia P.F. Araújo, Enhancing Inverse Halftoning via Coupled Dictionary Training, *Signa Processing : Image Communicatio* http://dx.doi.org/10.1016/j.image.2016.09.008

Enhancing Inverse Halftoning via Coupled Dictionary Training

Pedro G. Freitas[1,a], Mylène C.Q. Farias[b], Aletéia P.F. Araújo[a]

University of Brasília (UnB), Brasília, Brazil

[a] *Department of Computer Science*
[b] *Department of Electrical Engineering*

Abstract

Inverse halftoning is a challenging problem in image processing. Traditionally, this operation is known to introduce visible distortions into reconstructed images. This paper presents a learning-based method that performs a quality enhancement procedure on images reconstructed using inverse halftoning algorithms. The proposed method is implemented using a coupled dictionary learning algorithm, which is based on a patchwise sparse representation. Specifically, the training is performed using image pairs composed by images restored using an inverse halftoning algorithm and their corresponding originals. The learning model, which is based on a sparse representation of these images, is used to construct two dictionaries. One of these dictionaries represents the original images and the other dictionary represents the distorted images. Using these dictionaries, the method generates images with a smaller number of distortions than what is produced by regular inverse halftone algorithms. Experimental results show that images generated by the proposed method have a high quality, with less chromatic aberrations, blur, and white noise distortions.

Keywords: Coupled Dictionaries, Image Restoration, Inverse Halftoning, Enhancement, Training

1. Introduction

Printing a digital image requires a conversion from a digital representation to an analog representation. This process is often linked with digital halftoning, which is the technique of converting continuous-tone images into images with a limited number of tones (known as halftones) [1, 2]. The technique generates images that, although having a limited number of levels, convey the illusion of having a higher number of levels. Halftoning techniques can be applied both to grayscale and color images. On the other hand, inverse halftoning is the process of generating a reconstruction (or an approximation) of the original continuous-tone image from their halftoning versions. The inverse halftoning process is an important image restoration problem and is frequently associated with several other multimedia problems, such as content protection using watermarking [3], visual cyptography [4], compression of multimedia content [5], error concealment [6], and image quality assessment [7, 8].

Since halftoning techniques discard a considerable amount of information from the original continuous-tone image, distortions are frequently introduced in halftone images. As a consequence, the design of inverse halftoning techniques is challenging and, when compared to the original image, restored images may contain distortions. Most common distortions include color distortions, noise, or blur. Over the years, several inverse halftoning methods have been proposed. Examples include the works of Freitas *et al.* [9] and Saika *et al.* [10], who propose inverse halftoning methods that restore continuous-tone images from ordered dithering (OD) halftones. Xiong *et al.* [11], Kite *et al.* [12], and Neelamani *et al.* [13] propose wavelet-based approaches that restore images from halftones generated using error diffusion algorithms [14].

*Corresponding author
Email address: sawp@sawp.com.br (Pedro G. Freitas)

The aforementioned inverse halftoning techniques restore continuous-tone images using the knowledge about the specific halftoning technique used to produce the halftone (i.e. ordered dithering, error diffusion, dot diffusion, etc). However, in recent years, a few inverse halftoning techniques that work for different halftoning techniques have been proposed. One example is the work of Wen *et al.* [15] that uses a template optimization method (based on an elitist genetic algorithm) to implement a lookup-table inverse halftoning technique. Their method is able to restore Floyd-Steinberg error diffusion, Jarvis-Judice error diffusion, cluster dither, Bayer disperse dither, and dot diffusion halftone images. Another example is the work of Guo *et al.* [16] that is based on a block truncation code (BTC). Finally, Gopale and Sarode [17] propose a descreening inverse halftoning technique that uses image redundancy and adaptive filtering and does not require information about the halftoning process. Although these methods are state-of-the-art techniques, the continuous-tone images restored with them still present visual distortions, like for example noise and blur.

In this paper, we propose a new technique for effectively enhancing fine textures and details of restored halftone images, by concealing noise and blurring effects. More than yet another inverse halftoning algorithm, the technique aims to improve the results of existing inverse halftoning techniques. Practitioners of inverse halftoning algorithms can use it as a complementary step to improve the quality results obtained with their algorithm.

In the proposed technique, we consider the image restored with the inverse halftoning technique as a distorted version of the original image. Then, we use a coupled dictionary learning algorithm, which is based on a patchwise sparse representation. This approach was inspired by recent image restoration works that use coupled dictionary (CD) learning algorithms to improve the quality of distorted images [18]. For instance, Yang *et al.* [19] propose a CD training method for restoring images in single image super-resolution problems. Xiang *et al.* [20] attack the image deblurring problem using a CD learning framework. Reale *et al.* [21] identify thermal infrared face images from a gallery of visible light face images using CD.

Finally, it is worth mentioning the works of Son *et al.* [22, 23], who use CD to restore continuous tone images from their halftone version. Unlike Son's method, the method proposed in this paper is a technique for enhancing the visual quality of images restored using any inverse halftoning algorithm. In other words, the method has the goal of reducing the artifacts present in images restored by inverse algorithms.

The rest of this work is organized as follows. Section 2 contains a brief description of general halftone and inverse halftone algorithms. Section 3 presents the coupled dictionary learning model and the proposed methodology. Experimental results are reported in Section 4, while conclusions are presented in Section 5.

2. Halftoning and Inverse Halftoning

We consider the halftoning process as the technique of converting a continuous-tone grayscale image with 255 gray levels, I_g, into a binary black-and-white image with only two levels ('0' or '1'), I_b. More specifically,

$$I_b = \mathbf{f}(I_g), \tag{1}$$

where $\mathbf{f}$ is a function representing the halftoning algorithm. The function $\mathbf{f}$ can be computed using several mathematical models [24]. Each model corresponds to a unique dithering pattern strategy, which generates a different way of mapping the grayscale image I_g into the binary halftone I_b.

Inverse halftoning techniques are methods that reconstruct continuous-tone images from halftones. More formally, since $\mathbf{f}$ converts I_g to I_b, the inverse halftoning can be described as

$$I_g = \mathbf{f}^{-1}(I_b). \tag{2}$$

But, since the process of generating I_b discards a considerable amount of information, $\mathbf{f}$ is not injective and the inverse mapping is undefined. In other words, the reconstructed grayscale image is generated by approximating I_g and not by directly inverting the halftoning process. More specifically,

$$\hat{I}_g = I_g + \varepsilon, \tag{3}$$

where $\hat{I}_g$ is an approximation of the original grayscale image I_g generated by an inverse halftoning algorithm and ε is the approximation error that corresponds to a visible distortion.

The first row of Fig. 2 shows visual degradations (artifacts) corresponding to the distortion ε for different inverse halftoning techniques. Notice

that the type of visual distortion can vary according to the inverse halftoning technique. For example, color and noise artifacts may appear when using the Fast Inverse Halftoning Algorithm for Ordered Dithered Images (FIHT) [9] method to reconstruct the continuous-tones of each RGB channel. On the other hand, blur artifacts may appear when using Wavelet-based Inverse Halftoning via Deconvolution (WInHD) [13] or the Rolling guidance filter (RGF) [25] inverse halftoning techniques. Blur may also be introduced when using Local Approximations without (LASIP) or with (LASIPW) regularized inverse-regularized Wiener inverse [26].

In order to suppress these distortions, in this work, we use a technique to find the sparse representation shared by the original and the distorted images. As shown by Wright and Ma [27], the sparse representation of the images enables a linear relationships between non-distorted and distorted images. Therefore, it is possible to reconstruct an original image from its distorted version [28, 29]. The relationship between non-distorted and distorted images is learned using an unsupervised coupled dictionary (CD) learning approach to create two dictionaries of non-distorted and distorted image patches [30, 31]. In the next two sections, we describe the CD methodology and the inverse halftoning enhancement technique.

3. Inverse Halftoning Enhancement via Coupled Dictionary Learning

Given a distorted grayscale image $\hat{I}_g$, obtained from a halftone using an inverse halftoning algorithm, the enhancement problem consists of obtaining an image that best approximates the original image I_g. More specifically, these distortions of $\hat{I}_g$ are modeled as follows:

$$\hat{I}_g = \mathbf{SH}I_g, \tag{4}$$

where $\mathbf{S}$ and $\mathbf{H}$ represent the addition of blurring and noise distortions. These distortions were chosen because they are among the most commonly visible distortions found in images restored using inverse halftoning algorithms (see Fig. 2). The disadvantage of this model is that it is ill-posed. In other words, for a distorted image $\hat{I}_g$, there are several non-distorted images I_g that satisfy this constraint. We adapt this problem by dividing the non-distorted and distorted images, I_g and $\hat{I}_g$, into small patches x and y, respectively.

The patches x of non-distorted images can be represented as a linear combination of elements in the non-distorted images dictionary D_x. The dictionary is obtained in a training stage using sampled non-distorted patches. More specifically, x can be represented as follows:

$$x = D_x\alpha^*, \tag{5}$$

where $\alpha^* \in \mathbb{R}^k$ with $\|\alpha^*\|_0 \ll k$. In this case, α^* is the sparsest representation of x. In a similar way, α^* is also used to represent the patches y of the distorted image $\hat{I}_g$ with respect to other dictionary D_y. In this manner, both distorted (D_y) and non-distorted (D_x) dictionaries are trained to share the same sparse representation α^*.

3.1. Dictionary Learning

A straightforward strategy to generate the dictionaries D_x and D_y consists of sampling pairs $\{x_i^n, y_i^n\}$ of patches from I_g and $\hat{I}_g$, respectively. To preserve the correspondence between distorted and non-distorted information, we collect the patches from both distorted and non-distorted images at the same i-th spatial position. This naive strategy results in huge dictionaries which require a large amount of memory and processor resources.

To save computational resources, a sparse representation of the set of patches is used for dictionary training. In the literature, there are many approaches for finding dictionaries that guarantee the recovery of signals using sparse representations [31, 30, 32, 33]. In this paper, we use a learning-dictionary strategy that minimizes the differences between the signal and its sparse representation. In other words, we use the following optimization problem:

$$\begin{aligned} \arg\min_{D,\alpha} \quad & \|z - D\alpha\|_2^2 + \lambda\|\alpha\|_1 \\ \text{subject to} \quad & \|D_i\|_2^2 \leq 1, \end{aligned} \tag{6}$$

where $z = \{z_1, z_2, \cdots, z_i, \cdots, z_n\}$ is a set of n training samples, D_i is the i-th column of $\mathbf{D}$, λ is a constant that multiplies the ℓ_1 term (regularization parameter), and α is the sparse representation of z_i.

This optimization problem is not convex in both D and α, as previously demonstrated in other studies [34, 31]. However, it can be solved using an iterative strategy, which consists of finding the optimal α via linear programming [35] and then fixing

it to determine D via quadratic programming [34]. Otherwise, by fixing $\{\alpha_i\}$, $\mathbf{D}$ can be solved as a constrained quadratic problem [36]. This joint optimization problem converges to a local minimum [34].

3.2. Coupling Dictionaries

Although the strategy described in the previous section is efficient to represent z in terms of a dictionary, it is not able to tie the corresponding information of distorted and non-distorted patches. To achieve this, two dictionaries, D_x and D_y, must be learned in a way that guarantees that they share the same sparse representation α. An efficient strategy was proposed by Yang *et al.* [19]. In this strategy, sets of pairs $p = \{\{x_1, y_1\}, \{x_2, y_2\}, \cdots, \{x_n, y_n\}\}$ of non-distorted (x) and distorted (y) patches are sampled to create a common sparse representation. After extracting these pairs of patches, we can combine the individual sparse coding problems, i.e.,

$$\underset{D_x,\alpha}{\arg\min} \quad \|x - D_x\alpha\|_2^2 + \lambda\|\alpha\|_1 \tag{7}$$

and

$$\underset{D_y,\alpha}{\arg\min} \quad \|y - D_y\alpha\|_2^2 + \lambda\|\alpha\|_1, \tag{8}$$

to force them to share the same sparse representation as follows:

$$\begin{aligned} \underset{D_x,D_y,\alpha}{\arg\min} \quad & \|x - D_x\alpha\|_2^2 + \|y - D_y\alpha\|_2^2 + \lambda\|\alpha\|_1 \\ \text{subject to} \quad & \|D_{x_i}\|_2^2 \leq 1 \\ & \|D_{y_i}\|_2^2 \leq 1, \end{aligned} \tag{9}$$

or equivalently,

$$\begin{aligned} \underset{D_c,\alpha}{\arg\min} \quad & \|k_c - D_c\alpha\|_2^2 + \lambda\|\alpha\|_1 \\ \text{subject to} \quad & \|D_{c_i}\|_2^2 \leq 1, \end{aligned} \tag{10}$$

where $k_c = [x \;\; y]^\intercal$ and $D_c = [D_x \;\; D_y]^\intercal$ is the Coupled Dictionary (CD).

3.3. Inverse Halftoning Enhancement

After training the dictionaries D_x and D_y, corresponding to non-distorted and distorted training patches, we need to find a model for the image enhancement process. For this, we first extract the patches y from a distorted image $\hat{I}_g$, in the same way it was done during the training of the dictionaries. Then, for the i-th patch we find the sparse representation α with respect to D_y. This α is combined with D_x to generate the i-th non-distorted patch.

To find the sparse representation of y, we solve the following problem:

$$\begin{aligned} \min_{\alpha} \quad & \|\alpha\|_1 \\ \text{subject to} \quad & \|D_c\alpha - \tilde{y}\|_2^2 \leq \epsilon, \end{aligned} \tag{11}$$

where $\tilde{y} = [y \;\; w]^\intercal$ and w contains the values of the previously reconstructed non-distorted patches. After solving the above problem, we find the optimal solution for α^* (Eq. 5) to reconstruct the patch. After substituting all distorted $\{y_i\}$ patches by the corresponding non-distorted patches $\{x_i\}$, the image $\tilde{I}_g$ is reconstructed such that:

$$\tilde{I}_g = \hat{I}_g + \rho, \tag{12}$$

where $\rho < \varepsilon$ (see Eq. 3) and, therefore, $\tilde{I}_g$ is closer to the original image I_g than $\hat{I}_g$.

4. Experimental Results

The experiments were performed using a laptop with an Intel i7-4700MQ processor and 32GB of RAM running CentOS Linux 7. The code was implemented using Matlab R2015a. The training was first performed using two image databases. The first database is a set of texture images from the 'Texture' subset of the USC-SIPI Image Database [37]. These images have a single grayscale channel and dimensions equal to 512x512 or 1024x1024 pixels, with content varying from harsh to fine textures. The second database is the LIVE image quality database release 2 [38]. Since the results of the simulations were very similar for both databases, only the results of the USC-SIPI Image Database are reported in this paper.

The texture images of USC-SIPI database were converted into their halftone versions and the tested inverse halftoning algorithms were used to restore a continuous-tone grayscale image. Then, we collected the patch pairs from the original images and the restored images. These patches were randomly sampled from both sets of images, keeping a record of the spatial indexing corresponding to both original and restored information. These patch pairs were used for training the dictionaries following the learning steps described in Section 3. This training process was repeated for the following state-of-the-art inverse halftoning algorithms:

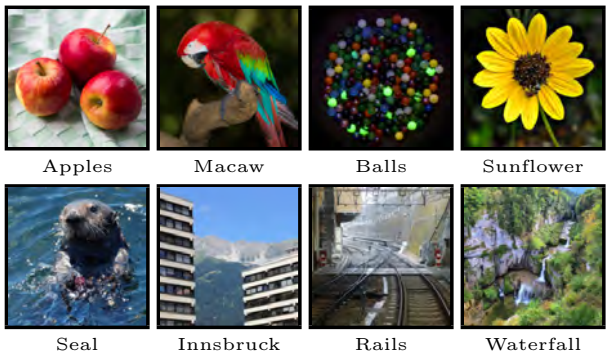

Figure 1: Original images used in the experimental tests.

FIHT [9], LASIP [26], LASIPW [26], RGF [25], and WInHD [13].

After training the dictionaries, we tested the proposed enhancing method using a set of colored images with different visual properties (content, color, frequency, and saliency), as depicted in Fig. 1. These images were collected from Wikipedia and are free of copyright, labeled for reuse with modification, and licensed under Creative Commons. Their original size is 512×512 pixels.

4.1. Enhancement Performance

To validate the proposed method, we first sampled 100,000 patches with size of 4x4 for training the pair of dictionaries D_x and D_y. We empirically set $\lambda = 0.2$ (see Eq. 10) and the size of the two dictionaries as 1024 atoms, what generally yields acceptable results.

Fig. 2 depicts a comparison of the output results obtained with our method for the aforementioned inverse halftoning algorithms. For all images, the first rows depict the results of the inverse halftoning algorithm and the second rows depict the results of their enhanced versions using CD. More specifically, Fig. 2-(a) shows details of each original image before the halftoning-and-inverse process. Fig. 2-(b), (c), (d), (e), and (f) show the restoration using FIHT, LASIP, LASIPW, RGF, and WInHD algorithms, respectively, without enhancement (1st row) and with enhancement using the proposed method (2nd row). From these images, we can notice that FIHT produces a noisier and sharper restoration, while the other algorithms produce blurry images. For all cases, we observe that distortions are minimized by using the proposed method.

The quality of these images is also measured objectively. First, we analyzed the fidelity between the reconstructed image and the corresponding original using the Peak Signal-to-Noise Ratio (PSNR). The first group of Table 1 depicts the PSNR values of the reconstructed images for different inverse halftoning algorithms and their enhancements using the proposed method. Even though PSNR is commonly used as an image quality metric, it is not actually reliable for rating visual image quality [39]. Taking this into consideration, we also use the Gradient Magnitude Similarity Deviation(GMSD) [40] and the Feature Similarity Index (FSIM) [41]. GMSD was chosen because it is a state-of-the-art metric that delivers a highly competitive prediction accuracy. On the other hand, FSIM is based on the fact that human visual system understands an image according to its low-level features. FSIM and GMSD scores of the reconstructed and enhanced images are shown in the second and third group of Table 1, respectively.

From Table 1, we can notice that the proposed method is able to enhance the quality of reconstructed images. However, in some cases, the enhancement algorithm has similar performance to the original inverse halftoning algorithms. This can be observed in the highlighted regions of Fig. 3. In this figure, the red color denotes the patches where sparse recovery enhances the inverse halftoning algorithms, the blue color denotes patches where the inverse halftoning algorithm (i.e. LASIP) beats the proposed algorithm, and the gray color indicates the patches where both behave similarly (the absolute RMSE difference between LASIP and LASIP+CD is smaller than 0.5). Interestingly, the proposed algorithm performs better on contour and high detail regions and worst on homogeneous regions. Furthermore, the regions where the proposed method works better coincide with the image salient regions [42].

Since inverse halftoning algorithms may introduce color distortions, in order to estimate the performance of the proposed algorithm, it is also important to estimate the strength of color distortions in reconstructed and enhanced images. In this work, we use the ΔE^* CIE color difference metric [43] to estimate the color fidelity of the reconstructed and enhanced images with respect to the original image. ΔE^* is a full reference color metric that estimates the distance between the colors in two images. In our experiments, we compute the ΔE^* for each image pixel and calculate the average

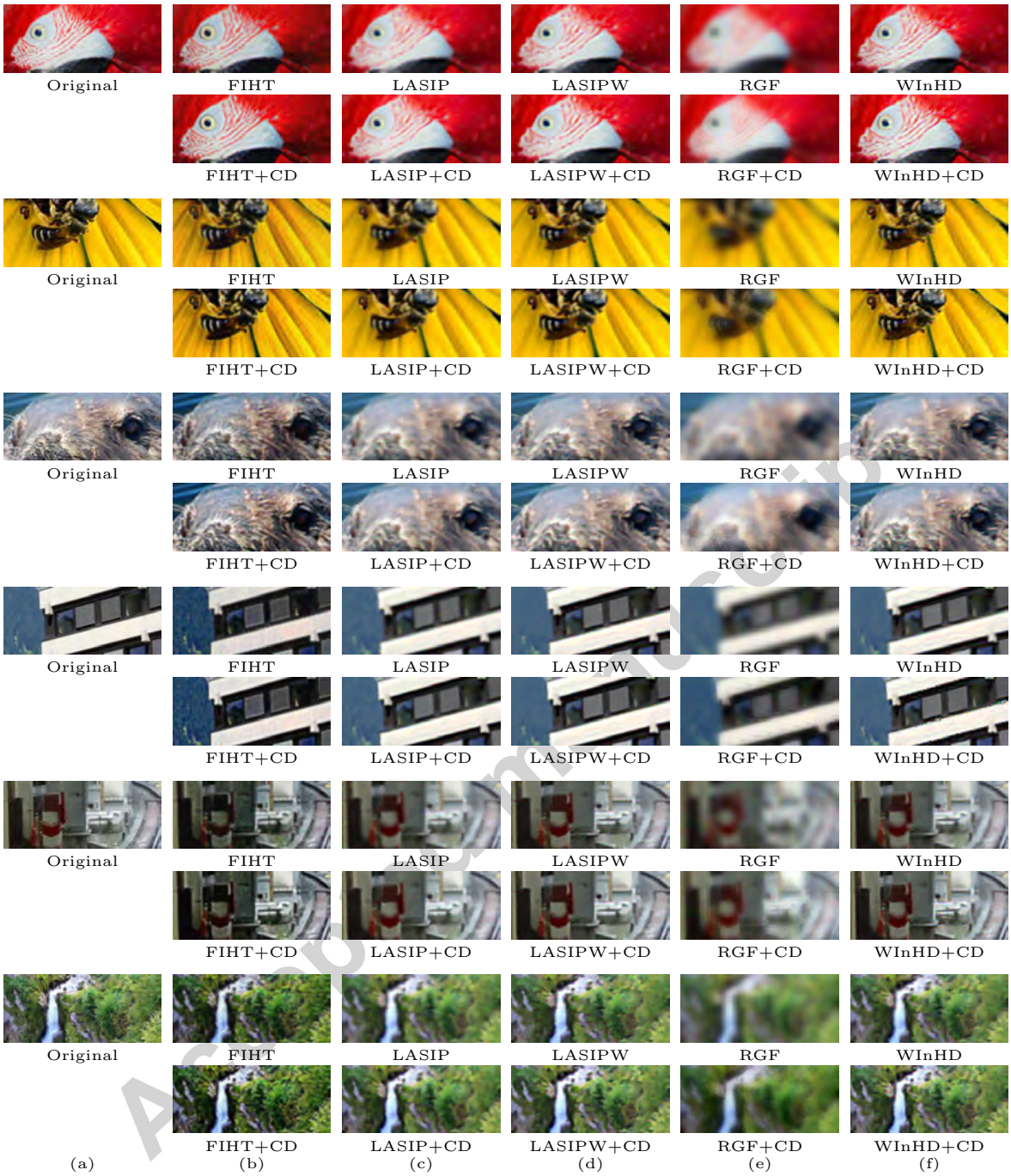

Figure 2: Examples of reconstructed images using different inverse halftoning techniques. From top to bottom: Macaw, Sunflower, Seal, Rails, and Waterfall.

value for the whole image, getting a single score for each image. Since ΔE^* is a distance metric, the smaller ΔE^* the better is the color quality of the reconstructed image. The fourth group of Table 1 shows the ΔE^* values. These values indicate that the proposed enhancement algorithm produces better results than using only the reconstruction algorithm.

Table 1: Objective evaluation of restoration and enhancement fidelity using PSNR, FSIM, GMSD, and ΔE^* quality metrics.

Metric	Method	Apples	Balls	Innsbruck	Macaw	Rails	Seal	Sunflower	Waterfall	Average
PSNR	FIHT	20.4558	24.2834	20.0043	21.6705	19.8340	19.1716	22.8609	20.0833	21.0455
	FIHT+CD	20.5425	24.2927	20.0281	21.7181	20.0285	19.2783	22.9233	20.3397	**21.1439**
	LASIP	34.8503	32.6038	28.3815	32.2517	26.6425	27.3351	29.4121	24.9422	29.5524
	LASIP+CD	34.9107	33.0873	29.0368	32.7689	27.3706	28.0053	30.3871	25.3020	**30.1086**
	LASIPW	34.3779	32.1201	28.8698	32.2838	27.3844	27.9374	29.5718	25.3399	29.7356
	LASIPW+CD	34.6645	32.5878	29.0814	32.4299	27.6205	27.9239	29.6811	25.5747	**29.9455**
	RGF	29.9674	27.0864	22.3269	27.6421	21.3362	22.4640	24.2723	20.7262	24.4777
	RGF+CD	30.1347	27.2315	22.7493	27.7821	21.3968	22.4477	24.6701	20.7365	**24.6436**
	WinHD	33.1707	29.5114	28.1179	31.0409	26.5176	27.5363	28.4972	25.0452	28.6797
	WinHD+CD	34.5786	30.3231	28.7520	31.4908	27.4606	27.8707	28.5945	25.4494	**29.3150**
FSIM	FIHT	0.9328	0.8803	0.9191	0.8972	0.9272	0.9409	0.9219	0.9513	0.9213
	FIHT+CD	0.9410	0.8817	0.9288	0.9019	0.9373	0.9502	0.9247	0.9597	**0.9282**
	LASIP	0.9819	0.9714	0.9481	0.9673	0.9588	0.9676	0.9609	0.9664	0.9653
	LASIP+CD	0.9826	0.9757	0.9589	0.9692	0.9702	0.9756	0.9667	0.9738	**0.9716**
	LASIPW	0.9795	0.9712	0.9506	0.9666	0.9653	0.9722	0.9633	0.9732	0.9677
	LASIPW+CD	0.9813	0.9756	0.9578	0.9694	0.9655	0.9712	0.9658	0.9725	**0.9699**
	RGF	0.9307	0.8922	0.7944	0.9062	0.7756	0.8138	0.8722	0.7855	0.8463
	RGF+CD	0.9336	0.8987	0.8115	0.9098	0.7757	0.8102	0.8804	0.7767	**0.8496**
	WinHD	0.9798	0.9659	0.9512	0.9676	0.9671	0.9719	0.9624	0.9733	0.9674
	WinHD+CD	0.9806	0.9705	0.9560	0.9680	0.9673	0.9734	0.9607	0.9746	**0.9689**
GMSD	FIHT	0.0801	0.1330	0.1044	0.0898	0.1053	0.0831	0.0807	0.0675	0.0930
	FIHT+CD	0.0765	0.1329	0.0993	0.0880	0.1022	0.0799	0.0805	0.0612	**0.0901**
	LASIP	0.0396	0.0498	0.0784	0.0602	0.0645	0.0505	0.0673	0.0519	0.0578
	LASIP+CD	0.0399	0.0493	0.0701	0.0594	0.0544	0.0437	0.0596	0.0440	**0.0525**
	LASIPW	0.0450	0.0601	0.0794	0.0665	0.0597	0.0492	0.0666	0.0443	0.0588
	LASIPW+CD	0.0428	0.0517	0.0750	0.0625	0.0595	0.0479	0.0634	0.0430	**0.0557**
	RGF	0.0865	0.1020	0.1817	0.1151	0.2106	0.1764	0.1608	0.1917	0.1531
	RGF+CD	0.0849	0.1047	0.1731	0.1150	0.2068	0.1720	0.1547	0.1852	**0.1495**
	WinHD	0.0447	0.0723	0.0842	0.0660	0.0592	0.0488	0.0745	0.0447	0.0618
	WinHD+CD	0.0427	0.0705	0.0780	0.0635	0.0571	0.0478	0.0664	0.0431	**0.0586**
ΔE^*	FIHT	8.0881	7.4621	8.3023	9.4527	8.8893	9.9822	7.8637	8.8652	8.6132
	FIHT+CD	8.0600	7.1777	8.2669	9.2131	8.9166	9.9479	7.7117	8.8822	**8.5220**
	LASIP	1.8752	2.6582	3.1945	2.5188	4.4409	3.6138	2.6212	5.4520	3.2968
	LASIP+CD	1.6837	2.4372	2.9816	2.2711	4.1390	3.3448	2.3953	5.2305	**3.0604**
	LASIPW	1.9313	3.0626	3.2666	2.5430	4.9916	4.0004	2.7671	5.9844	3.5684
	LASIPW+CD	1.7614	2.9223	3.1684	2.3578	4.8835	3.8531	2.6464	5.9668	**3.4450**
	RGF	2.8669	3.8693	4.6568	3.4845	6.1927	5.4156	4.0297	8.3631	4.8598
	RGF+CD	2.7102	3.6813	4.4286	3.2669	6.0805	5.2942	3.8296	8.2951	**4.6983**
	WinHD	1.8246	4.5780	3.4865	3.2724	4.9678	3.7485	3.8594	5.7593	3.9371
	WinHD+CD	1.7638	4.4548	3.3893	3.0935	4.9494	3.6818	3.6943	5.7476	**3.8468**

In order to verify the effect of regularization parameter λ, we vary it from 0.1 to 0.5 and repeat the procedure described in the last section using the LASIP inverse halftoning method. Table 2 shows the PSNR, FSIM, GMSD, and ΔE^* values obtained for five λ values in this interval. From this table, we can notice that the smaller the value of λ, the better the results. If we compare the average results of Table 2 with the results of the LASIP reconstruction without the enhancement (see Table 1), we can notice that the proposed method improves the quality of the reconstructed image when $\lambda < 0.4$. Larger

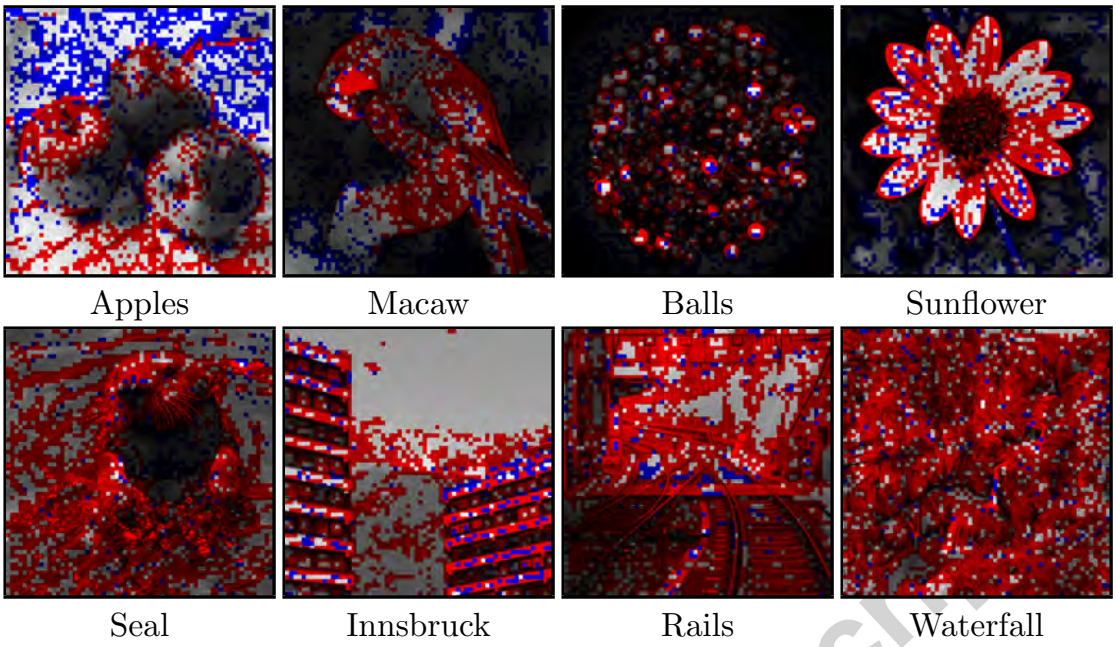

Figure 3: Comparison of enhancement between the original reconstruction using LASIP [26] inverse halftoning algorithm and the proposed method. Red blocks denotes patches where the proposed enhancement outperforms the original inverse halftoning algorithm. Blue blocks denotes patches where the proposed algorithm inserts noise and the original LASIP is superior. The gray areas of these images indicates that the two methods perform in a like manner.

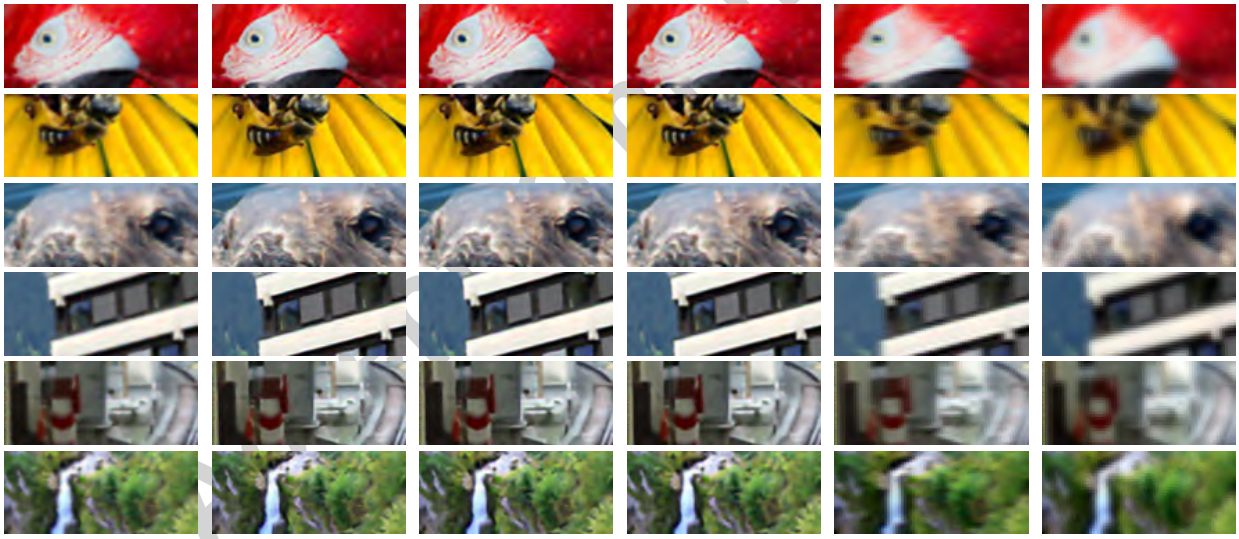

Figure 4: The effect of λ on the enhanced image given the restored image. From left to right: inverse halftoning reconstruction (LASIP), $\lambda = 0.1$, 0.2, 0.3, 0.4, and 0.5.

values of λ produce worse results. Fig. 4 shows the impact that different λ values have on image quality.

4.2. Computational Performance

The scalability of the learning stage is analyzed by varying the number of patches. As depicted in the bar-plot in Fig. 5, the time spent during the learning stage increases (linearly) with the num-

Table 2: Effect of regularization parameter on enhancement performance.

Metric	λ	Apples	Balls	Innsbruck	Macaw	Rails	Seal	Sunflower	Waterfall	Average
PSNR	0.1	34.7865	33.1051	29.2936	32.8036	27.4162	28.0692	30.7598	25.3020	**30.1920**
	0.2	34.7878	33.0259	29.1112	32.7161	27.4110	27.9891	30.5168	25.2139	30.0965
	0.3	34.7097	32.8966	28.8561	32.5450	27.1311	27.7111	30.2740	24.9551	29.8848
	0.4	32.1311	29.0823	25.5889	28.5804	22.9801	23.9100	25.8035	21.7816	26.2322
	0.5	30.5571	27.5080	22.7458	27.8700	21.6170	22.7020	24.4403	20.9673	24.8009
FSIM	0.1	0.9831	0.9771	0.9624	0.9709	0.9702	0.9753	0.9695	0.9730	**0.9727**
	0.2	0.9825	0.9763	0.9592	0.9691	0.9710	0.9763	0.9675	0.9743	0.9720
	0.3	0.9820	0.9757	0.9558	0.9680	0.9699	0.9760	0.9667	0.9737	0.9710
	0.4	0.9649	0.9390	0.9120	0.9367	0.8745	0.9025	0.9211	0.8709	0.9152
	0.5	0.9435	0.9076	0.8105	0.9188	0.7947	0.8323	0.8854	0.8045	0.8622
GMSD	0.1	0.0389	0.0476	0.0667	0.0578	0.0534	0.0434	0.0553	0.0445	**0.0509**
	0.2	0.0399	0.0508	0.0692	0.0602	0.0523	0.0427	0.0587	0.0430	0.0521
	0.3	0.0403	0.0519	0.0726	0.0609	0.0537	0.0434	0.0594	0.0439	0.0533
	0.4	0.0594	0.0722	0.1147	0.0974	0.1445	0.1168	0.1182	0.1428	0.1083
	0.5	0.0787	0.0938	0.1774	0.1134	0.1944	0.1598	0.1525	0.1724	0.1428
ΔE^*	0.1	1.6918	2.4389	2.9532	2.2712	4.1244	3.3352	2.3552	5.2120	**3.0477**
	0.2	1.6938	2.4509	2.9819	2.2797	4.1332	3.3440	2.3789	5.2606	3.0654
	0.3	1.7002	2.4639	3.0191	2.2925	4.1957	3.3937	2.4061	5.3714	3.1053
	0.4	1.9014	2.8603	3.5204	2.6208	5.4231	4.2964	3.0447	6.8758	3.8179
	0.5	2.0777	3.1358	4.2284	2.7489	6.1046	4.8446	3.4138	7.4063	4.2450

ber of samples. It is worth pointing out that the time values in this graph do not consider the time spent on 'file reading' and 'sampling' stages, which are approximately constant for all test images (130 seconds on average).

In order to estimate the overhead of the proposed enhancement, we varied the size of the images and the values of λ. The original images were resized from 16×16 to 2048×2048 pixels and, then, the halftoning, its inverse, and the enhancement steps were performed. The λ values ranged from 0.05 to 0.5 with steps of 0.05. These results are presented in Table 3. We can notice that the enhancement time increases with the image size. On the other hand, the higher the value of λ, the smaller the enhancing time. By comparing the results in Table 2 with the results in Table 3, we can conclude that the appropriate values for λ are in the range from 0.1 to 0.2.

4.3. Discussion

The implementation of the proposed method in this paper has some limitations that compromise its performance. First, the method was implemented using an unoptimized Matlab program (e.g. there are several code snippets that can be improved using vectorization resources instead of loops). Second, both training and restoration stages include patch-based operations (i.e., the processing of a given patch is independent of other patches). Given this independence between patches, the proposed method could have been implemented in parallel and used in real-time applications.

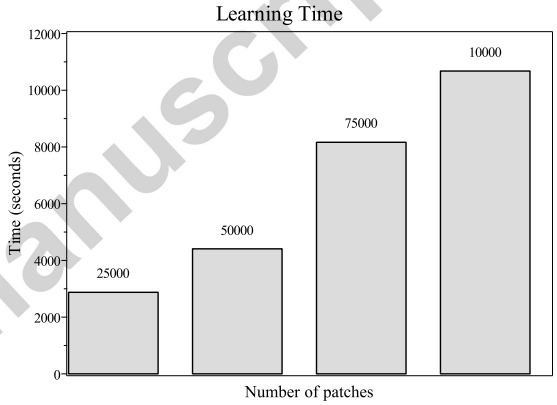

Figure 5: Computation time for learning dictionaries, in terms of the number of samples.

Although the method improves the quality of restored images, differences reported by regular quality metrics are small. It is worth pointing out that quality assessment of enhanced images is still a challenge [44, 45]. Examples of the poor performance of quality metrics for enhancement problems can be found in the work of Chang *et al.* [46]. Although Vu *et al.* [47] proposes a metric to assess the quality of images with contrast and brightness enhancements, this metric would not work for the images generated by the proposed method because they have a different type of enhancement.

The straightforward solution for assessing the quality of the enhanced images would be to construct a new database and, then, perform a psychophysical experiment to identify which tech-

Table 3: Average runtime (in seconds) for image enhancement, in terms of image spatial resolution and λ value.

	λ									
Size	0.05	0.1	0.15	0.2	0.25	0.3	0.35	0.4	0.45	0.5
16	0.163	0.110	0.106	0.103	0.102	0.098	0.085	0.078	0.075	0.073
32	1.210	0.798	0.724	0.525	0.469	0.402	0.319	0.258	0.258	0.258
64	5.289	3.171	2.458	2.100	1.893	1.621	1.312	1.092	1.077	1.077
128	19.055	12.435	9.899	8.541	7.705	6.770	6.605	6.428	6.426	6.054
256	78.272	47.696	46.786	42.725	35.355	33.116	30.147	29.009	29.301	28.001
512	280.872	179.606	154.014	144.039	139.613	122.245	117.847	115.407	111.794	102.709
1024	922.758	612.294	511.995	509.157	439.530	430.370	403.812	388.118	378.996	355.401
2048	3455.220	2070.507	1791.728	1773.035	1739.235	1689.187	1583.255	1421.524	1320.260	1358.376

niques has a better subjective quality. Nevertheless, the quality assessment of enhanced images requires a whole new study, which is out of scope of this paper.

5. Conclusions

This paper presented a method for improving the quality of images reconstructed using inverse halftoning algorithms based on coupled dictionaries. The dictionaries are trained considering the common sparse representation between the original images and the images reconstructed using inverse halftoning algorithms. The dictionary training (using a second dictionary) enforces that the sparsity derived from the restored images can be used to enhance their quality. Experimental results show that the proposed coupled dictionary approach is able to conceal distortions caused by inverse halftoning algorithms in high detailed regions. Future works include the implementation of a selective patch processing approach to apply the proposed enhancement strategy only to selected patches. Moreover, future works will also include an investigation for adapting the algorithm to be computed in parallel. Examples of the results can be found at the following address `http://tiny.cc/pbo7ey`.

Achnowledgment

This work was supported in part by Conselho Nacional de Desenvolvimento Cientfico e Tecnológico (CNPq), in part by Coordenação de Aperfeiçoamento de Pessoal de Nível Superior (CAPES), and in part by the University of Brasília (UnB).

References

[1] D. E. Knuth, Digital halftones by dot diffusion, ACM Transactions on Graphics (TOG) 6 (4) (1987) 245–273.

[2] C. M. Miceli, K. J. Parker, Inverse halftoning, Journal of Electronic Imaging 1 (2) (1992) 143–151.

[3] J. Ge, J. Pan, E. Fang, Application of digital watermarking technology to artistic screening image, in: Advanced Graphic Communications, Packaging Technology and Materials, Springer, 2016, pp. 187–196.

[4] M. Bharathi, R. Charanya, P. Student, T. Vijayan, Halftone visual cryptography & watermarking, International Journal of Engineering 2 (4).

[5] F. Ebner, P. McCandlish, Compression of grayscale image data using multi-bit halftoning, uS Patent 8,437,043 (May 7 2013).

[6] C. B. Adsumilli, M. C. Farias, S. K. Mitra, M. Carli, A robust error concealment technique using data hiding for image and video transmission over lossy channels, Circuits and Systems for Video Technology, IEEE Transactions on 15 (11) (2005) 1394–1406.

[7] N. Damera-Venkata, T. D. Kite, W. S. Geisler, B. L. Evans, A. C. Bovik, Image quality assessment based on a degradation model, Image Processing, IEEE Transactions on 9 (4) (2000) 636–650.

[8] Z. Shi, X. Wang, L. Fu, A method of color inverse halftoning image quality assessment based on image structural property, in: Advanced Graphic Communications, Packaging Technology and Materials, Springer, 2016, pp. 257–262.

[9] P. Freitas, M. Farias, A. de Araujo, Fast inverse halftoning algorithm for ordered dithered images, in: Graphics, Patterns and Images (Sibgrapi), 2011 24th SIBGRAPI Conference on, 2011, pp. 250–257. doi:10.1109/SIBGRAPI.2011.14.

[10] Y. Saika, K. Okamoto, F. Matsubara, Probabilistic modeling to inverse halftoning based on super resolution, in: Control Automation and Systems (ICCAS), 2010 International Conference on, 2010, pp. 162–167.

[11] Z. Xiong, M. T. Orchard, K. Ramchandran, Inverse halftoning using wavelets, Image Processing, IEEE Transactions on 8 (10) (1999) 1479–1483.

[12] T. D. Kite, N. Damera-Venkata, B. L. Evans, A. C. Bovik, A fast, high-quality inverse halftoning algorithm for error diffused halftones, Image Processing, IEEE Transactions on 9 (9) (2000) 1583–1592.

[13] R. Neelamani, R. Nowak, R. Baraniuk, Model-based inverse halftoning with wavelet-vaguelette deconvolution, in: Image Processing, 2000. Proceedings. 2000 International Conference on, Vol. 3, IEEE, 2000, pp. 973–976.

[14] N. Damera-Venkata, B. L. Evans, Adaptive threshold modulation for error diffusion halftoning, Image Processing, IEEE Transactions on 10 (1) (2001) 104–116.

[15] Z.-Q. Wen, Y.-L. Lu, Z.-G. Zeng, W.-Q. Zhu, J.-H. Ai, Optimizing template for lookup-table inverse halftoning using elitist genetic algorithm, Signal Processing Letters, IEEE 22 (1) (2015) 71–75.

[16] J.-M. Guo, H. Prasetyo, K. Wong, Halftoning-based

block truncation coding image restoration, Journal of Visual Communication and Image Representation 35 (2016) 193–197.

[17] A. M. Gopale, T. K. Sarode, Adaptive filtering a descreening approach for color scanned halftones, in: Advances in Computing, Communications and Informatics (ICACCI), 2015 International Conference on, IEEE, 2015, pp. 700–706.

[18] L.-W. Kang, C.-M. Yu, C.-Y. Lin, C.-H. Yeh, Image and video restoration and enhancement via sparse representation, Emerging Technologies in Intelligent Applications for Image and Video Processing (2016) 1.

[19] J. Yang, Z. Wang, Z. Lin, S. Cohen, T. Huang, Coupled dictionary training for image super-resolution, Image Processing, IEEE Transactions on 21 (8) (2012) 3467–3478.

[20] S. Xiang, G. Meng, Y. Wang, C. Pan, C. Zhang, Image deblurring with coupled dictionary learning, International Journal of Computer Vision 114 (2-3) (2015) 248–271.

[21] C. Reale, N. M. Nasrabadi, R. Chellappa, Coupled dictionaries for thermal to visible face recognition, in: Image Processing (ICIP), 2014 IEEE International Conference on, IEEE, 2014, pp. 328–332.

[22] C. Son, H. Park, Sparsity-based inverse halftoning, Electronics letters 48 (14) (2012) 832–834.

[23] C.-H. Son, H. Choo, Local learned dictionaries optimized to edge orientation for inverse halftoning, Image Processing, IEEE Transactions on 23 (6) (2014) 2542–2556.

[24] R. A. Ulichney, Review of halftoning techniques, in: Electronic Imaging, International Society for Optics and Photonics, 1999, pp. 378–391.

[25] Q. Zhang, X. Shen, L. Xu, J. Jia, Rolling guidance filter, in: Computer Vision–ECCV 2014, Springer, 2014, pp. 815–830.

[26] A. Foi, V. Katkovnik, K. Egiazarian, J. Astola, Inverse halftoning based on the anisotropic lpa-ici deconvolution, in: PROCEEDINGS OF THE 2004 INTERNATIONAL TICSP WORKSHOP ON SPECTRAL METHODS AND MULTIRATE SIGNAL PROCESSING, SMMSP 2004, 2004, pp. 49–56.

[27] J. Wright, Y. Ma, Dense error correction via-minimization, Information Theory, IEEE Transactions on 56 (7) (2010) 3540–3560.

[28] J. Wright, Y. Ma, J. Mairal, G. Sapiro, T. S. Huang, S. Yan, Sparse representation for computer vision and pattern recognition, Proceedings of the IEEE 98 (6) (2010) 1031–1044.

[29] D. L. Donoho, Compressed sensing, Information Theory, IEEE Transactions on 52 (4) (2006) 1289–1306.

[30] J. Mairal, F. Bach, J. Ponce, G. Sapiro, Online dictionary learning for sparse coding, in: Proceedings of the 26th Annual International Conference on Machine Learning, ACM, 2009, pp. 689–696.

[31] K. Kreutz-Delgado, J. F. Murray, B. D. Rao, K. Engan, T.-W. Lee, T. J. Sejnowski, Dictionary learning algorithms for sparse representation, Neural computation 15 (2) (2003) 349–396.

[32] S. Gao, I. W.-H. Tsang, L.-T. Chia, Sparse representation with kernels, Image Processing, IEEE Transactions on 22 (2) (2013) 423–434.

[33] Y. Chen, N. M. Nasrabadi, T. D. Tran, Hyperspectral image classification via kernel sparse representation, Geoscience and Remote Sensing, IEEE Transactions on 51 (1) (2013) 217–231.

[34] H. Lee, A. Battle, R. Raina, A. Y. Ng, Efficient sparse coding algorithms, Advances in neural information processing systems 19 (2007) 801.

[35] E. J. Candes, T. Tao, Decoding by linear programming, Information Theory, IEEE Transactions on 51 (12) (2005) 4203–4215.

[36] C. J. Albers, F. Critchley, J. C. Gower, Quadratic minimisation problems in statistics, Journal of Multivariate Analysis 102 (3) (2011) 698–713.

[37] A. G. Weber, The USC-SIPI image database version 5, USC-SIPI Report 315 (1997) 1–24.

[38] H. R. Sheikh, M. F. Sabir, A. C. Bovik, A statistical evaluation of recent full reference image quality assessment algorithms, IEEE Transactions on image processing 15 (11) (2006) 3440–3451.

[39] Z. Wang, A. C. Bovik, Mean squared error: love it or leave it? a new look at signal fidelity measures, Signal Processing Magazine, IEEE 26 (1) (2009) 98–117.

[40] W. Xue, L. Zhang, X. Mou, A. C. Bovik, Gradient magnitude similarity deviation: a highly efficient perceptual image quality index, IEEE Transactions on Image Processing 23 (2) (2014) 684–695.

[41] L. Zhang, L. Zhang, X. Mou, D. Zhang, Fsim: a feature similarity index for image quality assessment, Image Processing, IEEE Transactions on 20 (8) (2011) 2378–2386.

[42] M. C. Farias, W. Y. Akamine, On performance of image quality metrics enhanced with visual attention computational models, Electronics letters 48 (11) (2012) 631–633.

[43] G. Sharma, W. Wu, E. N. Dalal, The ciede2000 color-difference formula: Implementation notes, supplementary test data, and mathematical observations, Color Research & Application 30 (1) (2005) 21–30.

[44] D. M. Chandler, M. M. Alam, T. D. Phan, Seven challenges for image quality research, in: IS&T/SPIE Electronic Imaging, International Society for Optics and Photonics, 2014, pp. 901402–901402.

[45] D. M. Chandler, Seven challenges in image quality assessment: past, present, and future research, ISRN Signal Processing 2013.

[46] Z. Chen, T. Jiang, Y. Tian, Quality assessment for comparing image enhancement algorithms, in: 2014 IEEE Conference on Computer Vision and Pattern Recognition, IEEE, 2014, pp. 3003–3010.

[47] C. T. Vu, T. D. Phan, P. S. Banga, D. M. Chandler, On the quality assessment of enhanced images: A database, analysis, and strategies for augmenting existing methods, in: Image Analysis and Interpretation (SSIAI), 2012 IEEE Southwest Symposium on, IEEE, 2012, pp. 181–184.